Large Scale Left Ventricular Shape Atlas Using Automated Model Fitting to Contours

Pau Medrano-Gracia[1], Brett R. Cowan[1], David A. Bluemke[2], J. Paul Finn[3], João A.C. Lima[4], Avan Suinesiaputra[1], and Alistair A. Young[1]

[1] Anatomy with Radiology, University of Auckland, New Zealand
[2] National Institutes of Health Clinical Center, USA
[3] Diagnostic CardioVascular Imaging, University of California, USA
[4] Johns Hopkins Hospital, Johns Hopkins University, USA

Abstract. We demonstrate that large legacy databases of manually segmented cardiac MR images can be used to build a shape atlas based on 3D left-ventricular finite-element models. We make use of the Cardiac Atlas Project database to build an atlas of 2,045 asymptomatic cases from the MESA study. Manually placed anatomical landmarks on long-axis and short-axis magnetic resonance images were combined with manually drawn contours on the short axis images which were corrected for breath-hold mis-registration using an automated method. The contours were then fitted by the model using linear least squares optimisation. The fitting error was 0.5 ± 0.4 mm at end-diastole and 0.5 ± 0.6 mm at end-systole (mean $\pm$ std. dev.). Results were validated against 3D models created by experts in a sub-sample of 253 cases using manual breath-hold registration. The atlas surface error was 1.3 ± 0.8 mm at end-diastole and 1.2 ± 0.9 mm at end-systole. The end-diastolic volume error was 9.0 ± 8.7 ml; the end-systolic volume error was 0.8 ± 6.3 ml; and the mass error 5.9 ± 12.9 g. These differences arose mainly at the base and apex because long-axis images were used in the validation models, but were only used in the automated models to define basal fiducial markers. All models were aligned and scaled, and finally analysed by principal component analysis. Significant differences were found in the first mode shape (sphericity) by gender, smoking, and hypertension.

Keywords: Statistical Model, Cardiac Magnetic Resonance Imaging (MRI), Finite Element Modelling, Contour atlas.

1 Background

Cardiac magnetic resonance imaging (CMR) is routinely used to assess the human heart. CMR typically provides cines of a few long-axis (showing both apex and base) and several short-axis (cross-sections of the ventricle) planes.

However, high-quality 2D cross-sectional images are not enough to completely quantify the function and shape of the ventricles, hence the need for post-processing to define the endocardial and epicardial contours, and subsequent calculation of ejection fraction and other clinical parameters. A 3D finite-element

S. Ourselin, D. Rueckert, and N. Smith (Eds.): FIMH 2013, LNCS 7945, pp. 433–441, 2013.

model (FEM) of the left ventricle (LV) can accurately quantify both shape and function in a continuous fashion despite the discrete nature of the acquired data.

The cardiac cycle consists of many phases, of which the most important are end-diastole (ED), at the end of filling, and end-systole (ES) at the end of contraction. The cavity volume at these phases, EDV and ESV respectively, are important indicators of disease and are frequently used to quantify cardiac performance. The myocardial mass (LVM) is also important for diagnosis. All these features and their derivations (such as stroke volume, ejection fraction, wall thickening, etc.) are readily quantifiable from the FEM model.

Other 3D atlases of the LV that have been built in the literature include [1–6]. These authors have proposed different frameworks for building shape models from a relatively small number of subjects. To the best of our knowledge, this is the first attempt to construct an atlas of 2,000 finite element models based on a legacy database of manually defined contours. A finite element customization method using manual contours was developed in [7] and applied to 234 cases in [8], but that method did not account for breath-hold mis-registrations and did not accurately model the base (ventricles were horizontally cropped).

The contributions of this paper are: (1) the establishment of a large scale atlas of asymptomatic individuals, which is available at `www.cardiacatlas.org`; (2) development of a contour-registration framework (including a novel breath-hold correction algorithm) by which 3D FEMs are generated to constrain anatomical feasibility and error, (3) and demonstration of statistical variations in shape due to gender, hypertension, diabetes and smoking.

2 Methods

2.1 MESA Data

A total of 2,045 asymptomatic cases from the general population with no prior clinical evidence of cardiac disease, together with MRI images and manually drawn contours on the short axes at end-diastole and end-systole, were obtained with permission from the MESA cohort [9] through the Cardiac Atlas Project [10]. Images were acquired using gradient recalled echo cine MRI, with 10-12 short axis slices and one four chamber long axis slice (6 mm thickness, 4 mm gap, FOV 360-400 mm, 256x160 matrix, flip angle 20°, TE 3-5 ms, TR 8-10 ms) with 20-30 frames per slice. Each slice was acquired in a separate breath-hold acquisition. Contours were manually defined as a series of points by the MESA MRI core lab on short-axis slices for all cases at ED and ES [11] using Q-MASS software (v. 4.2, Medis, the Netherlands). For a typical case with 7-10 slices a total of $\approx 2,000$ contour points were available, covering most of the LV. The overall construction process for the atlas is shown in Fig. 1.

2.2 Fiducial Landmarks (All Models)

Fiducial landmarks were manually defined at the apex and base (2 points), the hinge points of the mitral valve (2 points), and at the insertions of the right

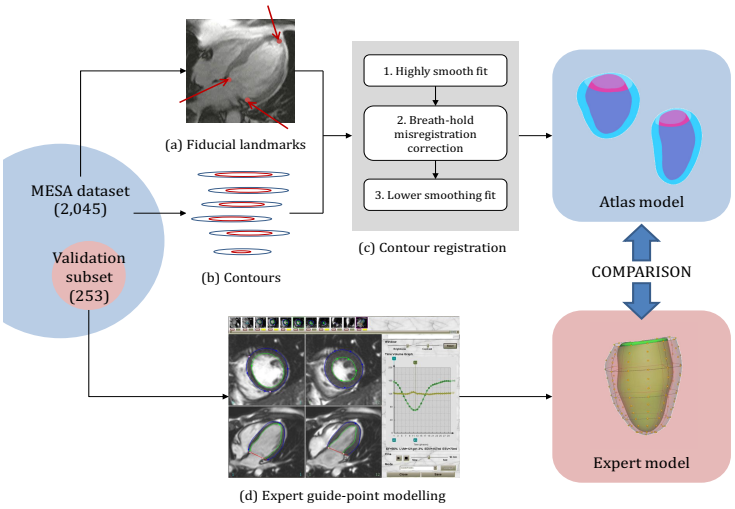

Fig. 1. Flow chart of the atlas construction: (a) Fiducial landmarks are defined (b) Contours were drawn on SA slices only (c) 3D models were derived from the contours (d) Expert guide-point modelling was employed in 12% of cases (validation dataset)

ventricular free wall into the inter-ventricular septum in the ED short axis images (1 point per short-axis slice). These were used to define the coordinate system and position of the initial model.

2.3 Atlas Construction

The initial model was formed by aligning and scaling an average generic model to the specific patient coordinate system and fiducial landmarks of each case. The contour points (after registration) were then automatically fitted by linear least squares to obtain the final model. Further, a 3D base plane was fitted in the long-axis direction to accurately represent the upper bound of the cavity at the mitral valve annulus.

Note that epicardial and endocardial contour data from the long-axis images was not included, since there were no manual contours available for the long axis images from the MESA laboratory.

The displacement in the λ-field (u) was fitted to introduce Sobolev smoothing [12] and was subject to a minimum wall thickness of $0.05\,\lambda$ units $\approx$ 1 mm. Therefore the objective function minimized was

$$E(u) = w\,S(u) + \sum_{g \in C} u_g^2 \quad \text{subject to} \quad \lambda_{\text{epi}} - \lambda_{\text{endo}} \geq 0.05 \tag{1}$$

where $S(u)$ represents the Sobolev smoothing, w the smoothing weight and u_g the displacement from the initial solution to the contour data point in element

coordinates. The summation spans across all available contour points ($g \in C$) except for those found above the base plane which were ignored. We minimised (1) as a quadratic programming problem using MATLAB's Optimisation Toolbox (v. 6.0, The MathWorks Inc., Natick, MA, USA).

If a case was encountered where the long-axis distance from the top contour to the base plane was greater than the thickness of 2 slices (approximately 20 mm), the case was omitted to minimise potential contamination of the atlas, since the fitting would be blind in these areas. This resulted in the exclusion of 9 cases (3.6%) in the validation dataset and 54 cases (2.6%) in the main dataset.

2.4 Breath-Hold Registration

Due to differences in breath-hold position between slices, the model can exhibit artefactual ripples in the longitudinal direction (Fig. 2(b)). Although breath-hold mis-registrations can result in arbitrary 3D rotations and translations for each slice, in practice these are well corrected by in-plane translations of the short axis images [13]. To correct the mis-registration, a three-step process was employed. Firstly, Eqn. 1 was solved using high stiffness weights ($w = 100$) to fit the uncorrected contours to provide a case-specific smooth version of the model. Secondly, the intersection of the image plane with the stiff model generated a new contour. From these pair of contours (the original and from the stiff model), an in-plane shift vector was defined between the centroids of the two contours, thus ensuring that the shifts aligned the contours to a coarse version of the anatomy. An average shift of 3.5 ± 2.5 mm was consistent with previously reported findings [13].

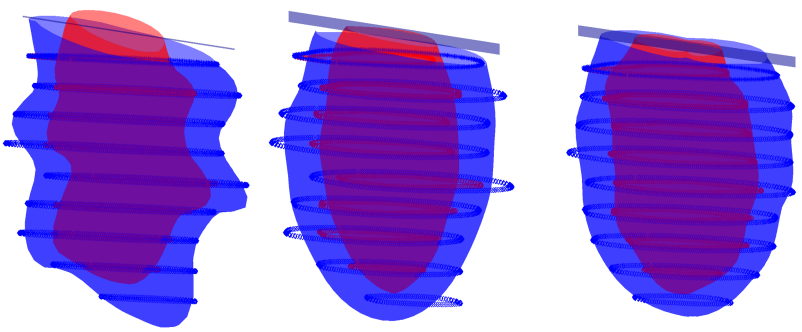

(a) (b) (c)

Fig. 2. Breath-hold correction: (a) original contours with a superimposed low-smoothness fit; (b) highly stiff model which serves as a guide for breath-hold correction; (c) final fit with low smoothness and corrected contours

Finally, another fit with the same constraints was performed with lower smoothing ($w = 1$). To improve the accuracy of the cavity volume, the final fit was also constrained to have the previously described mitral valve plane. This correction procedure ensured the preservation of the overall shape from the stiff fit, while minimising distortions in overall shape due to the registration procedure. An example case is shown in Fig. 2. The average computation time for a single case on a standard desktop (Intel® CPU Q6600, 2.4 GHz, RAM 4 GB) was ≈ 15 s per phase.

2.5 Validation

A random sample of 253 cases (12%) was independently analysed by experts using guide-point modelling [14] to produce models for validation of the automated process. Previously validated guide-point modelling [14] was used to adaptively optimise a time-varying 3D finite element model of the LV to fit each subject's images using custom software (CIM v. 6.0, Auckland, New Zealand). The model was defined in prolate spheroidal coordinates as $\lambda(\mu, \theta)$: a radial function of two angular coordinates [14]. In-plane shifting of the slices was manually applied by the expert to correct for breath-hold mis-registrations.

The model was interactively fitted to "guide points" provided by the analyst, as well as computer-generated data points calculated from the images using an edge detection algorithm. Note that the MESA contours were not used at all in the validation models; rather, the long and short axis images were analysed simultaneously to derive models directly from the images.

For the surface error, the atlas was sampled at evenly-spaced locations yielding 2,738 points. The Kabsch algorithm [15] (Procrustes superimposition) was pairwise applied (between corresponding *initial* and *expert-derived* cases) prior to the computation of this error to ensure maximum shape alignment between the validation model and automatic model.

For volume error (which is independent of coordinate systems), the endocardial cavity volume and the myocardial mass were analysed. Also, the overall surface error (or bias) was computed in a pair-wise fashion between the contour-fitted and validation models. All errors were computed as the validation model minus the automated model.

3 Results

The final-fit error between the contour points and the model surfaces from the 1,991 cases which survived missing data exclusion was (mean $\pm$ std.dev.) 0.5 ± 0.4 mm at end-diastole and 0.5 ± 0.6 mm at end-systole.

The atlas surface error, quantified in 253 cases between the automatic and validation models was 1.3 ± 0.8 mm at end-diastole and 1.2 ± 0.9 mm at end-systole. The end-diastolic volume error was 9.0 ± 8.7 ml; the end-systolic volume error was 0.8 ± 6.3 ml; and the mass error was 5.9 ± 12.9 g.

These errors were due primarily to differences at the apex and base because of the lack of long-axis contour information in the contour-derived models.

3.1 Statistical Modes

Principal component analysis (PCA) was used to analyse the modes of variation of the atlas. Given the non-Euclidean nature of the prolate spheroidal system used to describe the models, the statistical analysis was performed in Cartesian coordinates using 2,738 evenly-spaced sampled points per model. To be able to fairly assess shape variation irrespective of size or position, a Procrustes alignment to the mean was applied to all shapes, removing variation due to pose and scale.

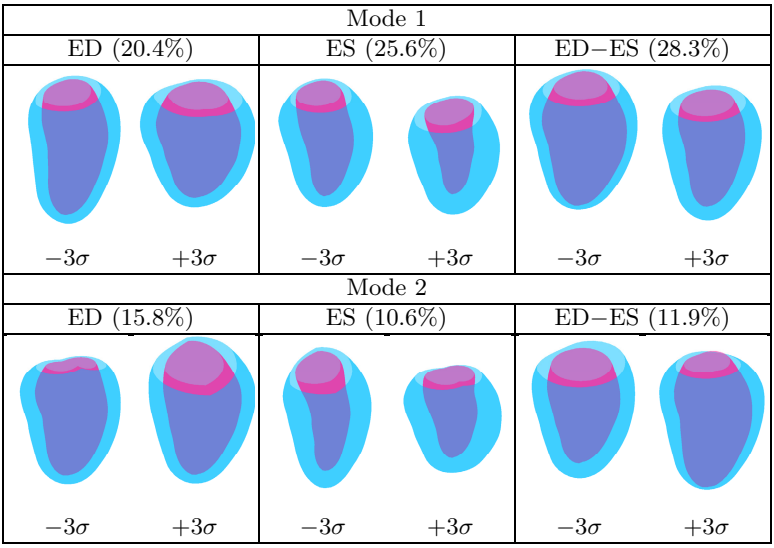

Fig. 3. PCA modes of variation of final atlas. Scale and position were removed by means of Procrustes alignment. Values in brackets are the represented power of variation.

Table 1. Statistical significance (p-values) of the mode weights in Fig. 3 for different subcohorts by means of unpaired two-tailed t-tests

		Mode 1			Mode 2		
	N	ED	ES	ED-ES	ED	ES	ED-ES
Hypertension (Y/N)	856/1135	**	0.52	0.19	*	***	0.23
Smoking (Y/N)	931/1053	*	****	****	*	0.40	0.91
Gender (M/F)	957/1034	***	***	***	0.42	0.15	0.86

$* = < 0.05$, $** = < 10^{-3}$, $*** = < 10^{-5}$, $**** = < 10^{-12}$.

Fig. 3 shows the first two modes of variation with their respective power for ED, ES and the coupled variation of ED−ES at $\pm 3\sigma$. This last mode can be described as a functional variation since it captures how the sample points vary from ED to ES (the difference is added to the mean ED shape). Lower modes are

available on-line (`www.cardiacatlas.org`). Having removed the size factor —which would otherwise appear as the first mode in all three configurations— the remainder of the variation primarily relates to the sphericity of the ventricle (e.g. Mode 1 for ED), the wall thickness (e.g. Mode 1 for ED-ES) and the geometry of the mitral valves (Mode 2). However, in general, these effects appeared coupled. This is because PCA retrieves global modes of variation and not localised effects that might cluster in regions of the LV [16].

The contribution of each mode to each case can be quantified by projecting to the dimensionally-reduced PCA space. The weights of this projection can be analysed according to external clinical data such as hypertension and smoking. Table 1 shows the statistical difference of these modal weights among sub-cohorts from the MESA dataset by means of unpaired two-tailed t-tests. Significant shape differences were associated with hypertension, smoking and gender; with diabetes showing no significant shape changes.

4 Discussion

We have demonstrated that it is possible to use large databases of contours to build an atlas in a semi-automatic fashion, using standard optimization methods. Fiducial markers and contours were placed manually but the rest of the steps for atlas formation —including breath-hold correction— were fully automatic. With the recent advent of fully automated landmark detection and contouring algorithms [17, 18] the entire atlas generation process could be automated. A particular feature of our algorithm was that special attention was directed to producing models which were always feasible by means of constraints in the optimisation.

Validation showed that the quality of the atlas is comparable to that of expert analysis except for where the lack of long-axis data impacted on the result (mainly at the apex). A variety of smoothing weights were tested for the stiff fits for correction of the breath-hold mis-registration and $w = 100$ gave the best compromise between removing high frequency oscillations but maintaining overall shape.

We have created one of the largest atlases of the left ventricle, built from 1,991 models. By analysing the static modes of variation, it is evident that sphericity, wall thickness and mitral valve geometry are the most important anatomical variations. The functional mode ED−ES also revealed the variability of ejection fraction.

Table 1 shows that there are significant shape differences associated with hypertension, smoking and gender. These require further investigation.

In the future, we plan to fully automate the atlas construction from MR images by incorporating automatic contour detection and automatic fiducial marker placement. This will enable us to generate even larger databases which in turn can be used to further refine these results.

Acknowledgements. The project described was supported by NIH (R01HL-087773). MESA was supported by contracts N01-HC-95159 through N01-HC-95169 from the NHLBI and by grants UL1-RR-024156 and UL1-RR-025005 from NCRR.

References

1. Lötjönen, J., et al.: Statistical shape model of atria, ventricles and epicardium from short- and long-axis MR images. MIA 8(3), 371–386 (2004)
2. Luo, H., O'Donnell, T.: A 3D statistical shape model for the left ventricle of the heart. In: Niessen, W.J., Viergever, M.A. (eds.) MICCAI 2001. LNCS, vol. 2208, pp. 1300–1301. Springer, Heidelberg (2001)
3. Medrano-Gracia, P., Cowan, B.R., Finn, J.P., Fonseca, C.G., Kadish, A.H., Lee, D.C., Tao, W., Young, A.A.: The Cardiac Atlas Project: preliminary description of heart shape in patients with myocardial infarction. In: Camara, O., Pop, M., Rhode, K., Sermesant, M., Smith, N., Young, A. (eds.) STACOM 2010. LNCS, vol. 6364, pp. 46–53. Springer, Heidelberg (2010)
4. Ordas, S., et al.: A statistical shape model of the heart and its application to model-based segmentation. In: SPIE Medical Imaging, vol. 6511 (2007)
5. Perperidis, D., Mohiaddin, R.H., Rueckert, D.: Construction of a 4D statistical atlas of the cardiac anatomy and its use in classification. In: Duncan, J.S., Gerig, G. (eds.) MICCAI 2005. LNCS, vol. 3750, pp. 402–410. Springer, Heidelberg (2005)
6. Rueckert, D., et al.: Automatic construction of 3-D statistical deformation models of the brain using nonrigid registration. IEEE-TMI 22(8), 1014–1025 (2003)
7. Lamata, P., et al.: An accurate, fast and robust method to generate patient-specific cubic hermite meshes. MedIA 15(6), 801–813 (2011)
8. Lewandowski, A., et al.: The preterm heart in adult life: Cardiovascular magnetic resonance reveals distinct differences in left ventricular mass, geometry and function. Circulation (2012)
9. Bild, D.E., et al.: Multi-ethnic study of atherosclerosis: objectives and design. Am. J. Epidemiol. 156, 871–881 (2002)
10. Fonseca, C.G., et al.: The Cardiac Atlas Project – an imaging database for computational modeling and statistical atlases of the heart. Bioinformatics 27(16), 2288–2295 (2011)
11. Yan, R.T., et al.: Regional left ventricular myocardial dysfunction as a predictor of incident cardiovascular events MESA (multi-ethnic study of atherosclerosis). Journal of the American College of Cardiology 57(17), 1735–1744 (2011)
12. Young, A., Hunter, P., Smaill, B.: Estimation of epicardial strain using the motions of coronary bifurcations in biplane cineangiography. IEEE Transactions on Biomedical Engineering 39(5), 526–531 (1992)
13. McLeish, K., et al.: A study of the motion and deformation of the heart due to respiration. IEEE-TMI 21(9), 1142–1150 (2002)
14. Young, A., et al.: Left ventricular mass and volume: Fast calculation with guidepoint modeling on MR images. Radiology 216(2), 597 (2000)
15. Kabsch, W.: A solution for the best rotation to relate two sets of vectors. Acta Crystallographica Section A 32, 922–923 (1976)

16. Üzümcü, M., Frangi, A.F., Sonka, M., Reiber, J.H.C., Lelieveldt, B.: ICA vs. PCA active appearance models: Application to cardiac MR segmentation. In: Ellis, R.E., Peters, T.M. (eds.) MICCAI 2003. LNCS, vol. 2878, pp. 451–458. Springer, Heidelberg (2003)
17. Lu, X., Georgescu, B., Jolly, M.-P., Guehring, J., Young, A., Cowan, B., Littmann, A., Comaniciu, D.: Cardiac anchoring in MRI through context modeling. In: Jiang, T., Navab, N., Pluim, J.P.W., Viergever, M.A. (eds.) MICCAI 2010, Part I. LNCS, vol. 6361, pp. 383–390. Springer, Heidelberg (2010)
18. Suinesiaputra, A., et al.: Left ventricular segmentation challenge from cardiac MRI: A collation study. In: Camara, O., Konukoglu, E., Pop, M., Rhode, K., Sermesant, M., Young, A. (eds.) STACOM 2011. LNCS, vol. 7085, pp. 88–97. Springer, Heidelberg (2012)